Robotica (2013) volume 31, pp. 549–554. © Cambridge University Press 2012
doi:10.1017/S0263574712000562

Optimal torque distribution method for a redundantly actuated 3-RRR parallel robot using a geometrical approach

Ho-Seok Shim†§, TaeWon Seo‡§ and Jeh Won Lee‡*

†*R & D Center, Pyung-Hwa Anti-Vibration Company, Daegu, 711-855, Republic of Korea*
‡*School of Mechanical Engineering, Yeungnam University, Gyeongsan 712-749, Republic of Korea*

(Accepted September 4, 2012. First published online: October 15, 2012)

SUMMARY

In this paper, a novel optimal torque distribution method for a redundantly actuated parallel robot is proposed. Geometric analysis based on screw theory is performed to calculate the stiffness matrix of a redundantly actuated 3-RRR parallel robot. The analysis is performed based on statics focusing on low-speed motions. The stiffness matrix consisting of passive and active stiffness is also derived by the differentiation of Jacobian matrix. Comparing two matrices, we found that null-space vector is related to link geometry. The optimal distribution torque is determined by adapting mean value of minimum and maximum angles as direction angles of null-space vector. The resulting algorithm is validated by comparing the new method with the minimum-norm method and the weighted pseudo-inverse method for two different paths and force conditions. The proposed torque distribution algorithm shows the characteristics of minimizing the maximum torque.

KEYWORDS: Torque distribution; Redundantly actuation; Parallel mechanism; Geometrical approach; Stiffness matrix, Screw theory.

1. Introduction

Redundant parallel robots have advantages of singularity avoidance and high stiffness compared with non-redundant robots.[1] Many redundant parallel robots have been proposed for various applications.[2–4] Kim *et al.*[5] proposed a redundant 6-degree of freedom (DOF) Eclipse-II mechanism, and actuator redundancy was used to avoid singularities inside the workspace. Jeong *et al.*[6] proposed a calibration algorithm for redundant parallel mechanisms. Muller[7] showed that backlash could be avoided by using redundant actuation based on inverse dynamics approach.

Since the number of actuators is greater than the number of degrees of freedom of redundantly actuated robots, there is no unique solution for actuator torques. Therefore, the actuator torques should be optimized with respect to operating conditions. There have been many studies of torque distribution methodology.[8–10] Kock and Schumacher[11] separated the operation torque into a minimum-norm torque and a null torque, and adjusted the null torque to change the system stiffness. However, a weighting in the null torque was selected manually during the procedure. Park *et al.*[12] applied a weighted pseudo-inverse method to a five-bar redundant parallel robot and obtained improved distribution results; however, the weighting selection was performed by trial-and-error.

The analysis of a parallel robot in screw coordinates has the advantages of geometric intuitiveness and produce simple equations. Duffy[13] and Griffis[14] are pioneers in the application of screw theory to parallel robots. They proposed kinematic, static, and dynamic modeling of a non-redundant parallel robot in screw coordinates. After reporting their parallel robot analysis based on screw theory, many other researchers, such as Mohamed and Gosselin,[15] Zhang,[16], and Moon *et al.*[17], proposed design methodologies for redundant parallel robots, 6-DOF parallel robot designs, and error compensation for parallel robots based on screw theory respectively. However, it is important to note that most of these studies are limited to a parallel robot with active prismatic joints.

In this study, a new optimal torque distribution method for a redundantly actuated parallel robot based on a geometric approach using screw theory is proposed. A planar parallel robot with three chains is composed of three revolute chains (the robot is named as "3-RRR" in this paper). A geometrical approach is introduced to set up the stiffness models of the parallel robot with revolute joints, which is more complicated to be analyzed than the parallel robot with prismatic joints. Based on the stiffness model, a simple torque distribution algorithm is proposed by considering geometrical characteristics. The proposed algorithm was validated using simulations on a circular path and a repeated linear path.

The rest of this paper is organized as follows. Section 2 describes the mechanism of the redundant 3-RRR parallel robot, and derived the stiffness matrix based on screw theory. Comparing with the stiffness matrix based on derivatives of Jacobian matrix, a new optimal torque distribution algorithm is proposed in Section 3. Section 4 presents simulation results for linear and circular path conditions. Our conclusions are presented in Section 5.

2. Stiffness Analysis of 3-RRR Parallel Robot

2.1. Mechanism description

Figure 1(a) shows the mechanism configurations of a 3-RRR parallel robot. The robot is operated by three actuators at

*Corresponding author. E-mail: jwlee@yu.ac.kr
§These authors (H.-S. Shim and T. Seo) made equal contributions as first author.

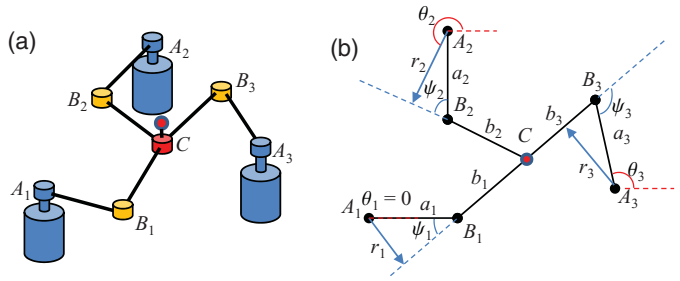

Fig. 1. (Colour online) Redundantly actuated 3-DOF planar parallel robot based on 3-RRR chains. (a) Mechanism description. (b) Schematic diagram of 3-RRR parallel robot. A_i and B_i denote the positions of actuators and moving R-joint, respectively, and C denotes the position of the end-effector. a_i and b_i denote the lengths of lines A_iB_i and B_iC respectively. r_i denotes the perpendicular distance from A_i to line B_iC. θ_i and ψ_i denote the angle of line A_iB_i and the angle between lines A_iB_i and B_iC ($i = 1, 2, 3$) respectively.

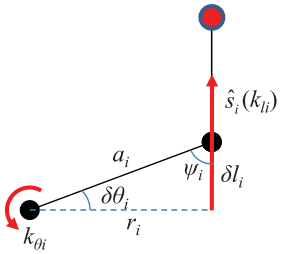

Fig. 2. (Colour online) Force lines in 3-RRR redundant parallel robot.

the base, and the revolute (R) joint is used to move the end-effector. This is a planar parallel mechanism whose mobility is 2. This type of mechanism is called a redundant actuation parallel mechanism. Figure 1(b) describes the parameters used in stiffness analysis based on screw theory. A detailed explanation of symbols is given along with the figure.

2.2. *Stiffness analysis*

The analysis is started by deriving wrench to the end-effector. The wrench of the 3-RRR redundantly actuated parallel robot is simply derived as follows[13]:

$$\hat{w} = \sum_{i=1}^{3} \frac{k_{\theta i}(\theta_i - \theta_{0i})}{r_i}\hat{s}_i = \sum_{i=1}^{3} \frac{k_{\theta i}(\theta_i - \theta_{0i})}{a_i \sin\psi_i}\hat{s}_i, \quad (1)$$

where $\hat{s}_i$ denotes unit screw vector in the direction of line B_iC, $k_{\theta i}$ is the rotational stiffness coefficient of the actuator, $(\theta_i - \theta_{0i})$ is the rotary displacement in each actuator, and ψ_i is the relative angle of the first link and the second link.

Next, the relation between the rotational stiffness coefficient ($k_{\theta i}$: the actuator stiffness coefficient) and the linear stiffness coefficient (k_{li}: the end-effector stiffness) is determined. The set up used to calculate the relation is shown in Fig. 2. The infinitesimal displacement in the linear direction (δl_i) is expressed as follows:

$$\delta l_i = r_i\delta\theta_i = a_i \sin\psi_i\delta\theta_i. \quad (2)$$

The relation between the force and the torque is given by

$$k_{li}r_i^2\delta\theta_i = k_{\theta i}\delta\theta_i. \quad (3)$$

From Eqs. (2) and (3), the relation between $k_{\theta i}$ and k_{li} is calculated as follows:

$$k_{li} = \frac{k_{\theta i}}{(a_i \sin\psi_i)^2}. \quad (4)$$

Then, substituting Eqs. (2) and (4) into Eq. (1) yields

$$\hat{w} = \sum_{i=1}^{3}\{k_{li}\,(l_i - l_{0i})\,\hat{s}_i\}, \quad (5)$$

where l_{0i} is the free length of the spring and l_i is the current length of the spring. Differentiating and rearranging Eq. (5) yields the following equation[13]:

$$\begin{aligned}
\delta\hat{w} &= \sum_{i=1}^{3}\{k_{li}\delta l_i\hat{s}_i\} + \sum_{i=1}^{3}\left\{k_{li}\,(l_i - l_{0i})\left(\frac{d\hat{s}_i}{d\theta_1}\right)\delta\theta_1\right\} \\
&= [\,\hat{s}_1\ \hat{s}_2\ \hat{s}_3\,]\,[k_l]\begin{bmatrix}\delta l_1\\ \delta l_2\\ \delta l_3\end{bmatrix} \\
&\quad + [\,\hat{s}_{1B}\ \hat{s}_{2B}\ \hat{s}_{3B}\,]\,[k_l(1-\rho)]\begin{bmatrix}l_1\delta\theta_1\\ l_2\delta\theta_2\\ l_3\delta\theta_3\end{bmatrix} \\
&= \left\{[\hat{s}_1\ \hat{s}_2\ \hat{s}_3]\begin{bmatrix}k_{l1} & 0 & 0\\ 0 & k_{l2} & 0\\ 0 & 0 & k_{l3}\end{bmatrix}\begin{bmatrix}\hat{s}_1{}^T\\ \hat{s}_2{}^T\\ \hat{s}_3{}^T\end{bmatrix} + [\,\hat{s}_{1B}\ \hat{s}_{2B}\ \hat{s}_{3B}\,]\right. \\
&\quad \left.\times\begin{bmatrix}k_{l1}\,(1-\rho_1) & 0 & 0\\ 0 & k_{l2}\,(1-\rho_2) & 0\\ 0 & 0 & k_{l3}\,(1-\rho_2)\end{bmatrix}\begin{bmatrix}\hat{s}_{1C}{}^T\\ \hat{s}_{2C}{}^T\\ \hat{s}_{3C}{}^T\end{bmatrix}\right\}\delta\hat{D}.
\end{aligned} \quad (6)$$

where $\delta l_i = \hat{s}_i{}^T\delta\hat{D}$, $l_i\delta\theta_i = \hat{s}_{iC}{}^T\delta\hat{D}$, and $\hat{s}_{iB}$ and $\hat{s}_{iC}$ ($i = 1, 2, 3$) denote the unit screw vectors that are perpendicular to $\hat{s}_i$ and are passing through joints B and C respectively. Duffy[13] (p. 148–152) explained in detail the description of perpendicular screw vectors. ρ_i is the rational displacement of l_{0i}/l_i, and $\delta\hat{D}$ is the infinitesimal displacement of the end-effector position C. Equation (6) can be simplified as follows:

$$\delta\hat{w} = \left\{\boldsymbol{J}_l\,[k_l]\,\boldsymbol{J}_l^T + [B]\,[k_l\,(1-\rho)]\,[C]^T\right\}\delta\hat{D} = [K]\delta\hat{D}, \quad (7)$$

where $\boldsymbol{J}_l$ is a Jacobian matrix consisting of screw vectors $[\hat{s}_1\ \hat{s}_2\ \hat{s}_3]$, $[B]$ and $[C]$ are matrices consisting of the vectors $[\,\hat{s}_{1B}\ \hat{s}_{2B}\ \hat{s}_{3B}\,]$ and $[\,\hat{s}_{1C}\ \hat{s}_{2C}\ \hat{s}_{3C}\,]$, which are perpendicular to $\hat{s}_i$ in matrix $\boldsymbol{J}_l$. $[k_l]$ and $[k_l\,(1-\rho)]$ are 3×3 diagonal matrices of stiffness coefficients.[13] In this study, since the mechanism has only two translational mobility, $\boldsymbol{J}_l$, $[B]$, and $[C]$ matrices are assumed as 2×3 matrices.

https://doi.org/10.1017/S0263574712000562 Published online by Cambridge University Press

3. Optimal Torque Distribution

In this section, the proposed optimal torque distribution algorithm is described. First, the fundamental derivation of the external force and the torques is presented. Then the algorithm is derived based on screw theory.

3.1. Fundamentals of torque distribution

In redundant parallel robot systems, the force on the end-effector ($\vec{F}_c$) can be uniquely determined from the actuator torques ($\vec{\tau}_\mathrm{A}$) as follows:

$$\vec{F}_c = \boldsymbol{J}^T \vec{\tau}_\mathrm{A}, \tag{8}$$

where $\boldsymbol{J}$ is a 2×3 Jacobian matrix of the redundant system. Note that $\boldsymbol{J}$ can be calculated from $\boldsymbol{J}_l$ in Eq. (7) from the definition of Jacobian as follows:

$$\begin{aligned}\boldsymbol{J} &= \begin{bmatrix} \|\vec{a}_1 \times \vec{b}_1\| & 0 & 0 \\ 0 & \|\vec{a}_2 \times \vec{b}_2\| & 0 \\ 0 & 0 & \|\vec{a}_3 \times \vec{b}_3\| \end{bmatrix}^{-1} \begin{bmatrix} \vec{b}_1{}^T \\ \vec{b}_2{}^T \\ \vec{b}_3{}^T \end{bmatrix} \\ &= \begin{bmatrix} r_1 & 0 & 0 \\ 0 & r_2 & 0 \\ 0 & 0 & r_3 \end{bmatrix}^{-1} \begin{bmatrix} \vec{b}_1{}^T \\ \vec{b}_2{}^T \\ \vec{b}_3{}^T \end{bmatrix} \equiv \boldsymbol{P}^{-1} \boldsymbol{J}_l{}^T, \end{aligned} \tag{9}$$

where $\vec{a}_i$ and $\vec{b}_i$ denote Cartesian link vectors of links a_i and b_i respectively. $\boldsymbol{P}$ is used for [diag(r_i)], where r_i is a moment arm for the end-effector. Note that $[\vec{b}_1\ \vec{b}_2\ \vec{b}_3]$ is equal to $J_l (= [\hat{s}_1\ \hat{s}_2\ \hat{s}_3])$. Note that $\vec{b}_i$ is the same as the screw vector ($\hat{s}_\mathrm{i}$), since $\vec{b}_i$ represents the directional vector of last links. Here the torque distribution problem can be determined to calculate proper $\vec{\tau}_\mathrm{A}$ when $\vec{F}_c$ is given. In Eq. (8), the Jacobian matrix is not a square matrix in a redundant system; therefore, there is no unique solution of $\vec{\tau}_\mathrm{A}$ for a given $\vec{F}_c$. The indefinite actuator torques are calculated as follows:

$$\vec{\tau}_A = (\boldsymbol{J}^T)^+ \vec{F}_c + (\boldsymbol{I} - (\boldsymbol{J}^T)^+ \boldsymbol{J}^T) Z, \tag{10}$$

where $(\boldsymbol{J}^T)^+$ denotes the pseudo-inverse of $\boldsymbol{J}^T$, which is equal to $\boldsymbol{J}(\boldsymbol{J}^T \boldsymbol{J})^{-1}$. $\boldsymbol{I}$ is the unit matrix and Z is an arbitrary vector which can change torque without affecting the end-effector force.

A. Minimum-norm torque distribution: The simplest way to distribute torques in a redundant system is the minimum-norm torque distribution method. First, the first term on the right-hand side (RHS) of Eq. (10) is defined as the minimum-norm torque, and the second term as the null-space torque. The minimum-norm torque method only uses the minimum-norm torque to control the redundant system. The proposed method[11] uses a pseudo-inverse least-squares method, and has an advantage that the internal force between links can be minimized. However, the drawback of this method is that differences between the magnitudes of actuator torques are increased.

B. Weighted pseudo-inverse method: The weighted pseudo-inverse method[12] applies a weighting factor to the minimum-norm torque as follows:

$$\vec{\tau}_{AW} = (\boldsymbol{J}^T)^{W+} \vec{F}_c = \boldsymbol{W}^{-1} \boldsymbol{J} (\boldsymbol{J}^T \boldsymbol{W}^{-1} \boldsymbol{J})^{-1} \vec{F}_c, \tag{11}$$

where the weighting matrix (W) is defined by a diagonal matrix of each weight of diag(w_i). The weighted pseudo-inverse method gives better results than the minimum-norm torque method by varying the weights. Various studies have been performed by selecting weights with the magnitude of minimum-norm torque or squares of consumption coefficients.[12–18] However, it is not clear which value of weight gives the best performance for a redundant system; thus, research is ongoing.

C. Null-space method: The null-space method is a torque-distribution method[11] that changes $\vec{\tau}_\mathrm{A}$ by a null-space torque of $(\boldsymbol{I} - (\boldsymbol{J}^T)^+ \boldsymbol{J}^T) Z$. The method has more degrees of freedom to control actuator torques by varying the arbitrary vector Z. However, choosing the arbitrary vector Z to improve the performance of a redundant system is a remaining problem. Recently, Lee *et al.*[8] selected the null-space vector which can make the desired shape of a compliance ellipsoid. Kim *et al.*[19] selected the null-space vector Z, which can generate arbitrarily reduced torque limit. The algorithm used in our research is based on the null-space method by choosing a proper vector Z. In this research, a simple and efficient method is proposed to choose vector Z by using a geometrical approach. The detailed procedure is described in Section 3.2.

3.2. Torque distribution algorithm by geometrical approach

The stiffness matrix of a redundant mechanism is calculated from actuator stiffness and torque. The relationship between actuator torques and stiffness of the end-effector in task coordinates is as follows[11]:

$$[K] = \boldsymbol{J}^T [k_a] \boldsymbol{J} + \boldsymbol{H}^T (\vec{\tau}_m + \beta \vec{\tau}_t), \tag{12}$$

where $[k_a]$ is a 3×3 diagonal matrix of actuator stiffness of diag (k_i), and $\boldsymbol{H}$ is a Hessian matrix defined by $\boldsymbol{H}^T = \delta \boldsymbol{J}^T / \delta D$ (D is the displacement of end-effector). $\vec{\tau}_m$ is the minimum-norm torque, and $\vec{\tau}_t$ is the null-space torque. In redundant systems, the 2×2 stiffness matrix $[K]$ can be changed by changing the constant β. Changing stiffness means that the actuator torques are changed without changing the external force. In Eq. (12), the first term describes the passive stiffness, which depends on the position of a link and actuator stiffness. The second term describes the active stiffness, which can be changed by an appropriate choice of a null-space torque vector. Comparison of Eqs. (7) and (12) reveals that the first term of $[K]$ looks identical in form but the second term of $[K]$ looks different. If the second term of $[K]$ in Eq. (7) is converted to the same form as Eq. (13), the second term of $[K]$ in Eq. (12) can be divided into minimum-norm torque and a null-space torque terms. The second term of $[K]$ in Eq. (7) can be expanded as

https://doi.org/10.1017/S0263574712000562 Published online by Cambridge University Press

$$
\begin{aligned}
&[B]\,[k_l\,(1-\rho)]\,[C]^T \\
&= [\,\hat{s}_{1B}\ \hat{s}_{2B}\ \hat{s}_{3B}\,] \\
&\quad \times \begin{bmatrix} k_{l1}\,(1-\rho_1) & 0 & 0 \\ 0 & k_{l2}\,(1-\rho_2) & 0 \\ 0 & 0 & k_{l3}\,(1-\rho_2) \end{bmatrix} \begin{bmatrix} \hat{s}_{1C}{}^T \\ \hat{s}_{2C}{}^T \\ \hat{s}_{3C}{}^T \end{bmatrix} \qquad (13) \\
&= \hat{s}_{1B} k_{l1}\,(1-\rho_1)\,\hat{s}_{1C}{}^T + \hat{s}_{2B} k_{l2}\,(1-\rho_2)\,\hat{s}_{2C}{}^T \\
&\quad + \hat{s}_{3B} k_{l3}\,(1-\rho_3)\,\hat{s}_{3C}{}^T \\
&= k_{l1}\hat{s}_{1B}\hat{s}_{1C}{}^T + k_{l2}\hat{s}_{2B}\hat{s}_{2C}{}^T + k_{l3}\hat{s}_{3B}\hat{s}_{3C}{}^T - \rho_1 k_{l1}\hat{s}_{1B}\hat{s}_{1C}{}^T \\
&\quad - \rho_2 k_{l2}\hat{s}_{2B}\hat{s}_{2C}{}^T - \rho_3 k_{l3}\hat{s}_{3B}\hat{s}_{3C}{}^T,
\end{aligned}
$$

where $k_{li}\hat{s}_{iB}\hat{s}_{iC}{}^T$ and $\rho_i k_{li}\hat{s}_{iB}\hat{s}_{iC}{}^T$ $(i = 1, 2, 3)$ are calculated as follows:

$$
k_{li}\hat{s}_{iB}\hat{s}_{iC}{}^T = k_{li}\frac{\delta\hat{s}_i}{\delta\theta_i}\frac{l_i\delta\theta_i}{\delta D} = k_{li}l_i\frac{\delta\hat{s}_i}{\delta D},
$$

and

$$
k_{li}\rho_i\hat{s}_{iB}\hat{s}_{iC}{}^T = k_{li}\frac{l_{0i}}{l_i}\frac{\delta\hat{s}_i}{\delta\theta_i}\frac{l_i\delta\theta_i}{\delta D} = k_{li}l_{0i}\frac{\delta\hat{s}_i}{\delta D}. \qquad (14)
$$

Inserting results of Eq. (14) in Eq. (13) yields

$$
\begin{aligned}
[B]\,[k_l\,(1-\rho)]\,[C]^T &= \sum_{i=1}^{3}\frac{\delta\hat{s}_i}{\delta D}(k_{li}l_i - k_{li}l_{0i}) \\
&= \frac{\delta}{\delta D}[\hat{s}_1\ \hat{s}_2\ \hat{s}_3]\begin{bmatrix} k_{l1}l_1 - k_{l1}l_{01} \\ k_{l2}l_2 - k_{l2}l_{02} \\ k_{l3}l_{i3} - k_{l3}l_{03} \end{bmatrix} \\
&= \frac{\delta \boldsymbol{J}_l}{\delta D}[k_{li}l_i - k_{li}l_{0i}]. \qquad (15)
\end{aligned}
$$

Finally, from the definition of Hessian matrix $\frac{\delta \boldsymbol{J}^T}{\delta D} = \boldsymbol{H}^{\mathbf{T}}$ and $\boldsymbol{J} = \boldsymbol{P}^{-1}\boldsymbol{J}_l^T$ in Eq. (9), $[K]$ in Eq. (7) can be written in a form similar to that of Eq. (12) as follows:

$$
\begin{aligned}
[K] &= \boldsymbol{J}_l\,[k_l]\,\boldsymbol{J}_l^T + [B]\,[k_l\,(1-\rho)]\,[C]^T \qquad (16) \\
&= \boldsymbol{J}^T\boldsymbol{P}^T\,[k_l]\,\boldsymbol{P}\boldsymbol{J} + \frac{\delta \boldsymbol{J}^T\,[r_i]^T}{\delta D}[-k_{li}l_{0i} + k_{li}l_i] \\
&= \boldsymbol{J}^T\boldsymbol{P}^T\,[k_l]\,\boldsymbol{P}\boldsymbol{J} + \boldsymbol{H}^T[-k_{li}l_{0i}r_i + k_{li}l_i r_i] \\
&\equiv \boldsymbol{J}^T\,[k_a]\,\boldsymbol{J} + \boldsymbol{H}^T(\vec{\boldsymbol{\tau}}_{l0i} + \vec{\boldsymbol{\tau}}_{li}).
\end{aligned}
$$

Comparing Eq. (16) with Eq. (12) yields information about the torques. $\vec{\tau}_{l0i}$ in Eq. (16) represents the nominal torque from the position of the end-effector, which is the same as the minimum-norm torque $\vec{\tau}_m$ in Eq. (12). $\vec{\tau}_{li}$ in Eq. (16) corresponds to the null-space torque $\beta\vec{\tau}_t$ in Eq. (12) since term $k_{li}l_i r_i$ cannot affect the end-effector force. Therefore, in a geometric sense, the null-space torque can be changed by l_i and r_i since k_{li} is a constant. From Eq. (2), l_i is also a dependent parameter of r_i; therefore, the null-space torque can be considered to be a torque that depends on the magnitude of r_i. The geometrical meaning of r_i is a perpendicular distance from the actuation point to the second link as shown in Fig. 3.

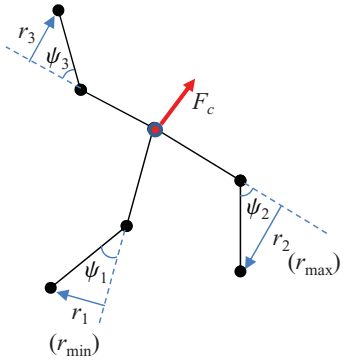

Fig. 3. (Colour online) Relationship between the force line and the generated torque.

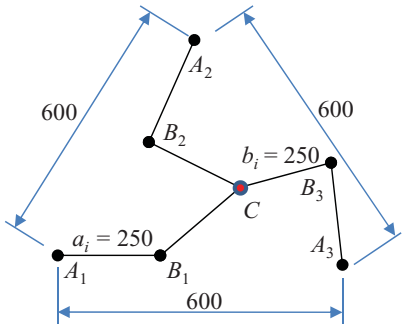

Fig. 4. (Colour online) Kinematic parameters of a redundant 3-RRR parallel robot to be used in simulation.

Assume that r_2 is the maximum value and r_1 is the minimum value among three distances in Fig. 3. The actuator torques are determined by the end-effector force $\vec{F}_c$. In order to make the magnitude of torques to have less difference between each other, the maximum actuator torque τ_2 must be decreased and the minimum actuator torque τ_1 must be increased. Here the key idea is the changing of directions of $\hat{s}_1$ and $\hat{s}_2$ to make r_1 equal to r_2; the mean value of ψ_1 and ψ_2 is the new direction of screw vector $\hat{s}_n$. By this process, the new direction of the screw vector $\hat{s}_n$ is selected as the null-space vector Z in Eq. (10). It is important to note that changing direction of the screw coordinate does not mean changing the actual link geometry; rather, it means changing the virtual link geometry for torque distribution with a smaller deviation.

4. Simulations

The proposed torque distribution algorithm was validated by simulation using MATLAB® software (Version R2009b, MathWorks, Natick, MA, USA). The dimensions of the 3-RRR redundant parallel mechanism for the simulation are shown in Fig. 4. The results of the minimum-norm method,[11] the weighted pseudo-inverse method,[12] and the proposed

https://doi.org/10.1017/S0263574712000562 Published online by Cambridge University Press

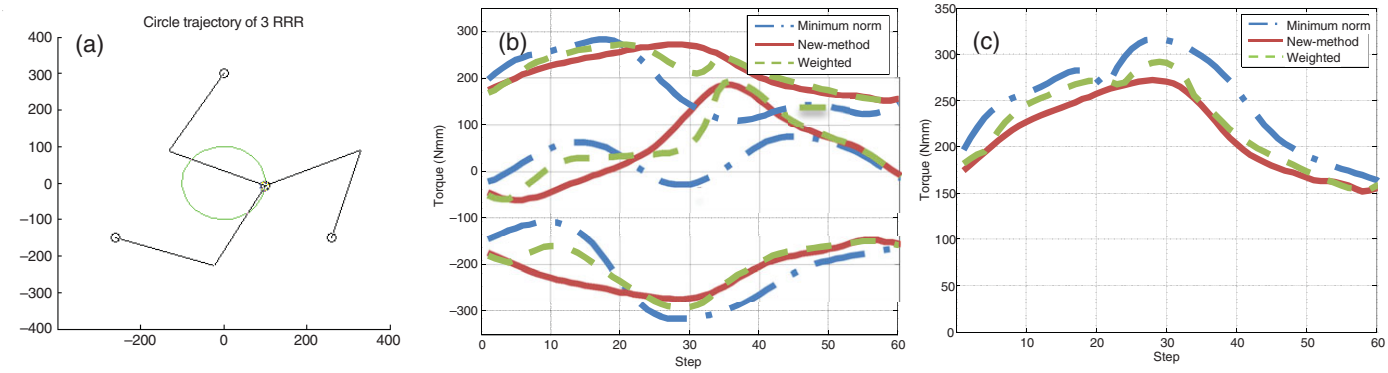

Fig. 5. (Colour online) (a) Circular path trajectory, (b) operation torques of each actuator, and (c) minmax value.

method based on a geometrical approach were compared. In order to calculate torques of each actuator, the minimum-norm torque method used $\boldsymbol{\tau}_m = (J^T)^+ \vec{F}_c$ from Eq. (10). The weighted pseudo-inverse method used Eq. (11) with minimum-norm torques as weighting matrix. The proposed method used Eq. (10) with new null-space vector Z, which is obtained from angle $\psi_{\text{virtual}} = (\psi_{\max} + \psi_{\min})/2$. Since there are three actuators, the minimum values of maximum torque are compared because the deviation of maximum and minimum values of torques should be reduced,

$$\text{minmax}\,(\tau_i) = \min(\max(|\tau_1|\,, |\tau_2|\,, |\tau_3|). \qquad (17)$$

4.1. *Circular path*

First, the results of the minimum-norm method,[11] the weighted pseudo-inverse method,[12] and the proposed method based on a geometrical approach along a circular path were compared. The analysis was performed based on statics, and the dynamic effects were not considered. Each actuator torque was calculated while an external force is applied to the end-effector along pre-defined path of the end-effector. As the end-effector moved along a circular path with a diameter of 100 mm, an external force of $F_c = [11]\,N$ was applied to the end-effector. Figure 5(a) shows the circular path trajectory. Figure 5(b) shows the calculated torques of each actuator for the minimum-norm method, the weighted pseudo-inverse method, and the proposed method based on the geometrical approach. Figure 5(c) shows the minmax (τ_i) value of each method. The proposed method (shown by the red solid line) generated the most regulated torque among three methods.

4.2. *Repeated linear path*

This 3-RRR mechanism can be used for the mechanism of an automobile haptic shift.[20] Repeated linear path resembles an automobile shift path. In this case, the external force direction is different for each path as $F_{c1} = [10]$ N, $F_{c2} = [0 - 1]$ N, $F_{c3} = [-10]$ N, and $F_{c4} = [0 - 1]$ N. Figure 6(a) shows the repeated linear path trajectory of simulation, and Figs. 6(b) and (c) show the results of simulation. The analysis was also performed based on static relation in Section 3. As expected, the proposed method based on the geometrical approach gave the best results among the three methods.

4.3. *Simulation results*

The simulation results of the three methods are compared and summarized in Table I. The proposed methods show improvement of 14.05% and 27.04% compared with the minimum-norm method, and improvement of 6.85% and 2.97% compared with the weighted pseudo-inverse method for circular and linear paths respectively. The results show that the proposed algorithm had a good effect on minimizing the maximum torque to follow the trajectory. The results also show that the proposed method based on the geometrical approach gives a torque profile of lower deviation for various user conditions as shown in Figs. 5 and 6.

In ref. [21], many other cases that include different paths and link configurations are simulated. The result was that

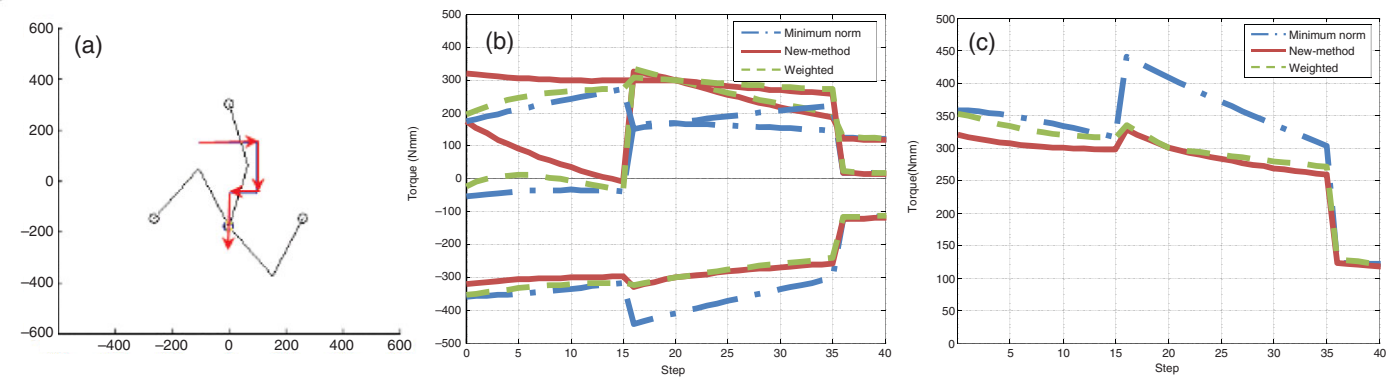

Fig. 6. (Colour online) (a) Repeated linear path trajectory, (b) operation torques of each actuator, and (c) minmax value.

https://doi.org/10.1017/S0263574712000562 Published online by Cambridge University Press

Table I. Comparison of minmax values by minimum-norm method, weighted pseudo-inverse method, and proposed method based on geometrical approach (unit: N·mm).

	Minimum-norm	Weighted pseudo-inverse	Proposed method
Circular path	316.36	291.93	271.94
Repeated linear path	440.79	357.59	346.97

the proposed method shows the least maximum torque. The torque minimization methodology is useful for the prevention of actuator saturation and actuator downsizing.

5. Conclusion

A redundantly actuated parallel robot has the infinite torque set for the same work. The minimum-norm torque which uses pseudo-inverse of Jacobian matrix minimizes the Euclidian norm of all actuator torques but makes large deviation between maximum and minimum torques. Through redistribution of the maximum torque, we can use a small motor for economic efficiency. Torque distribution method is closely related to stiffness matrix manipulation method. Stiffness matrix is derived by screw vectors. This paper shows that stiffness matrix based on screw geometry has analogy to stiffness matrix based on derivatives of Jacobian matrix. Stiffness matrix-based derivatives of Jacobian matrix consist of passive stiffness, which depends on the position of link and actuator stiffness and the active stiffness which can be changed by an appropriate choice of a null-space torque vector. This paper shows that a null-space torque vector is geometrically related to r_i, which is a perpendicular distance from actuator to line vector of the second link. The proposed algorithm is geometrically intuitive and there is no need for selection of arbitrary constants, which are the main drawbacks of previous algorithms. Simulations with different paths and forces were performed to validate the proposed algorithm. The maximum torque is decreased at most by 27% compared with the minimum-norm method, and by 6% compared with the weighted pseudo-inverse method.

The proposed method is applied to a planar mechanism. To extend this algorithm to a spatial mechanism, geometrical characteristics of spatial mechanisms should be clearly defined. This research remains as a future work for the proposed algorithm.

Acknowledgments

This research was supported by Yeungnam University Research Grant in 2007. The authors gratefully acknowledge this support.

References

1. J. Wang, J. Wu, T. Li and X. Liu, "Workspace and singularity analysis of a 3-DOF planar parallel manipulator with actuation redundancy," *Robotica* **27**, 51–57 (2008).
2. J. Callardo-Alvarado, R. Lesso-Arroyo and J. Santos-Miranda, "A worm-inspired new spatial hyper-redundant manipulator," *Robotica* **29**(4), 571–579 (2011).
3. J. Kim, F. C. Park, S. J. Ryu, J. Kim, J. Hwang, C. Park and C. Iurascu, "Design and analysis of a redundantly actuated parallel mechanism for rapid machining," *IEEE Trans. Robot. Autom.* **17**(4), 423–434 (2001).
4. T. Seo, D. S. Kang, H. S. Kim and J. Kim, "Dual servo control of a high-tilt 3-DOF micro parallel positioning platform," *IEEE-ASME Trans. Mechatronics* **14**(5), 616–25 (2009).
5. J. Kim, J.-C. Hwang, J.-S. Kim, C. C. Iurascu, F. C. Park and Y. M. Cho, "Eclipse-II: a new parallel mechanism enabling continuous 360-degree spinning plus three-axis translational motions," *IEEE Trans. Robot. Autom.* **18**(3), 367–373 (2002).
6. J. Jeong, D. Kang, Y. M. Cho and J. Kim, "Kinematic calibration for redundantly actuated parallel mechanism," *J. Mech. Des. Trans. ASME*, **126**(2), 307–318 (2004).
7. A. Muller, "Internal preload control of redundantly actuated parallel manipulators – its application to backlash avoiding control," *IEEE Trans. Robot.* **21**(4), 668–677 (2005).
8. S. Lee, S. Kim, W. In, M. Kim, J. I. Jeong and J. Kim, "Experimental verification of antagonistic stiffness planning for a planar parallel mechanism with 2-DOF force redundancy," *Robotica* **27**(4), 547–554 (2011).
9. S. B. Nokleby, R. Fisher, R. P. Podhorodeski and F. Firmani, "Force capabilities of redundantly actuated parallel manipulators," *Mech. Mach. Theory*. **40**(5), 578–599 (2005).
10. W. S. Owen, E. A. Croft and B. Benhabib, "Acceleration and torque redistribution for a dual-manipulator system," *IEEE Trans. Robot.* **21**(6), 1226–1230 (2005).
11. S. Kock and W. Schumacher, "A parallel x-y manipulator with actuation redundancy for high-speed and active-stiffness applications," *IEEE Int. Conf. Robot. Autom.* **3**, 2295–2300 (1998).
12. D. I. Park, S. H. Lee, S. H. Kim and Y. K. Kwak, "Torque distribution using a weighted pseudoinverse in a redundantly actuated mechanism," *Adv. Robot.*, **17**, 807–820 (2003).
13. J. Duffy, *Statics and Kinematics with Application to Robotics* (Cambridge University Press, Cambridge, UK, 1996).
14. M. W. Griffis, "Kinestatic Control: A Novel Theory for Simultaneously Regulating Force and Displacement," *Ph.D. Dissertation* (University of Florida, Gainesville, FL, 1991).
15. M. G. Mohamed, C. M. Gosselin, "Design and analysis of kinemtically redundant parallel manipulators with configurable platforms," *IEEE Trans. Robot*. **21**(3), 277–287, (2005).
16. B. Zhang, "Design and Implementation of a 6-DOF Parallel Manipulator with Passive Force Control," *Ph.D. Dissertation* (University of Florida, Gainesville, FL, 2005).
17. S.-K. Moon, Y. M. Moon, S. Kota and R. G. Landers, "Screw theory-based metrology for design and error compensation of machine tools," **In**: *Proceedings of ASME Design Engineering Technology Conferences*, **1**, 1–11, Pittsburgh, PA (Sep. 9–12, 2001).
18. M. Honegger and A. Codourey, "Redundancy resolution of a Cartesian space operated heavy industrial manipulator," In: *Proceedings of the IEEE International Conference on Robotics and Automation*, May 16–20 (Springer, Berlin, Germany, 1998) pp 2094–2098.
19. T.-J. Kim, B.-J. Yi and I. H. Suh, "Load distribution algorithms and experimentation for a redundantly actuated, singularity-free 3-DOF parallel haptic device," In *Proceedings of the IEEE/RSJ International Conference*, Sep. 28–Oct. 2 (Springer, Berlin, Germany, 2004) pp. 480–486.
20. S.-M. Woo, "Development of Haptic Interface for Shift by Wire of Intelligent Automobile" *MS Thesis* (Yeungnam University, Republic of Korea, 2008).
21. H.-S. Shim, "Optimal Torque Distribution Method of Redundant 3-RRR Parallel Robot by Geometrical Analysis," *Ph.D. Thesis* (in Korean) (Yeungnam University, Republic of Korea, 2009).